



Molecular dynamic simulation study of the structural anisotropy in $\text{Cu}_{50}\text{Zr}_{50}$ and $\text{Cu}_{64.5}\text{Zr}_{35.5}$ metallic glasses induced by static uniaxial loading within the elastic regime

Y. Zhang^{a,*}, N. Mattern^a, J. Eckert^{a,b}

^a IFW Dresden, Institute for Complex Materials, Helmholtzstr. 20, D-01069 Dresden, Germany

^b TU Dresden, Institute of Materials Science, D-01062 Dresden, Germany

ARTICLE INFO

Article history:

Received 3 July 2010

Received in revised form 11 October 2010

Accepted 27 October 2010

Available online 4 November 2010

Keywords:

Metallic glasses

Structural anisotropy

Elastic deformation

ABSTRACT

The structural anisotropy in both $\text{Cu}_{50}\text{Zr}_{50}$ and $\text{Cu}_{64.5}\text{Zr}_{35.5}$ metallic glasses induced by various static uniaxial loads within the elastic regime was studied by molecular dynamic simulations. Constant tensile and compressive loads from zero up to 200 MPa below the flow stress were applied in the simulation. The degree of anisotropy was characterized using a second order contact fabric tensor. It is found that the degree of anisotropy within the elastic regime increases with the applied load following an exponential growth function. The most part of the structural anisotropy can be attributed to the Zr–Cu atomic pairs in $\text{Cu}_{64.5}\text{Zr}_{35.5}$ and Zr–Cu, Cu–Cu atomic pairs in $\text{Cu}_{50}\text{Zr}_{50}$. The evolution of the structural anisotropy associated with the Zr–Zr and Cu–Cu pairs exhibits complex behavior, which implies that the deformation mechanism and the dynamics of $\text{Cu}_{50}\text{Zr}_{50}$ and $\text{Cu}_{64.5}\text{Zr}_{35.5}$ metallic glasses under compressive loads may be quite different from those under tensile loads.

© 2010 Elsevier B.V. All rights reserved.

1. Introduction

Metallic glasses (MGs) have been long thought as structurally isotropic since there is no long range order in these materials comparing to their crystalline counterparts. However, structural anisotropy (SA) has been observed in plastically deformed MGs by careful conventional X-ray [1] or synchrotron diffraction experiments. Dmowski and Egami [2] studied the SA in a $\text{Fe}_{81}\text{B}_{13}\text{Si}_4\text{C}_2$ MG induced by mechanical creep deformation. The SA was clearly shown by the difference in the intensities between two measuring geometries. Révész et al. [3] reported the SA in a $\text{Zr}_{57}\text{Ti}_5\text{Cu}_{20}\text{Al}_{10}\text{Ni}_8$ bulk metallic glasses induced by high pressure torsion under room temperature. The shift of the first halo position of the structure factor can be clearly observed on both the surface and the cross section of the deformed samples. It is well known that the plastic deformation of metallic glass are highly inhomogeneous under low temperature and high strain rates [4]. The inhomogeneous plastic flow is mostly localized within very tiny shear bands with sizes of about 5–10 nm [5]. It is, therefore, very straightforward to associate the SA introduced by plastic deformation with the formation of the shear bands. Nevertheless, SA can also be introduced by deformation within the elastic regime, where no obvious shear bands appear in the deformed sample. Mat-

tern et al. [6] studied the structural evolution of $\text{Cu}_{50}\text{Zr}_{50}$ and $\text{Cu}_{64.5}\text{Zr}_{35.5}$ MGs upon uniaxial tensile deformation using *in situ* synchrotron diffraction, where the shift of the first peak of both the structure factor and the pair correlation function has been clearly demonstrated.

Meanwhile, there are many studies on the atomic structure [7–12] and SA of Cu–Zr MGs using molecular dynamic (MD) simulations. Tomida and Egami simulated the SA introduced by deformation under constant loading using two models [13]: one was a single-component glass with a modified Johnson potential and the other was a two-component glass with a Lennard-Jones potential. The SA was demonstrated using a sixth-order spherical-harmonic component. It was suggested that the SA caused by anelastic deformation was dominated by the bond-reorientation process. Recently, it was reported by Rountree that the SA in an amorphous silica induced by shear deformation can be conveniently characterized by the fabric tensor method using MD simulation [14].

Notwithstanding many efforts to reveal the SA in MGs, reliable results on SA significantly rely on sophisticated experiments and data analysis methods since the introduced SA is normally minute. Meanwhile, the study of the SA in MG system is not widely carried out. Nevertheless, the evidence of the presence of SA even within the elastic regime is very important, since the SA may be related with the early stage of the formation of shear bands or the activation of the shear transformation zones. An accurate characterization of SA is therefore very helpful both to underpin the understanding of

* Corresponding author. Tel.: +49 351 4659 686; fax: +49 351 4659 452.
E-mail address: yue.zhang@ifw-dresden.de (Y. Zhang).

the mechanism of SA and to control the deformation behavior of MGs.

In this work, the SA of $\text{Cu}_{50}\text{Zr}_{50}$ and $\text{Cu}_{64.5}\text{Zr}_{35.5}$ MGs induced by static uniaxial loading (compressive and tensile) under room temperature is studied using MD simulations. The SA is characterized using a second order contact fabric tensor (FT) and the anisotropic coefficient. The contributions to the SA of different atomic pairs (Zr–Zr, Zr–Cu and Cu–Cu) are studied.

2. Simulation and methods

The simulation boxes of $\text{Cu}_{50}\text{Zr}_{50}$ and $\text{Cu}_{64.5}\text{Zr}_{35.5}$ contain 3000 atoms. Since there is no intention to study the plastic deformation, we believe that such box size is adequate to achieve both good statistic resolution and optimum computation time. The initial configurations of $\text{Cu}_{50}\text{Zr}_{50}$ and $\text{Cu}_{64.5}\text{Zr}_{35.5}$ were constructed using a random distribution of Cu and Zr atoms in a cubic simulation box according to the stoichiometry. The potential reported by Kim and Lee [15] using the embedded atom method (EAM) was employed and periodical boundary conditions was used. The NPT ensemble was used throughout the simulation process, i.e. the temperature and pressure were controlled by the Nose/Hoover thermostat and barostat with the external pressure setting to be zero. The simulation step size was set to be 2 fs.

The constructed $\text{Cu}_{50}\text{Zr}_{50}$ and $\text{Cu}_{64.5}\text{Zr}_{35.5}$ simulation boxes were melt at 2200 K for 200 ps and then were cooled down to 300 K continuously. After the target temperature of 300 K was reached, the boxes were relaxed for 1 ns before any load was applied. The relaxation processes were performed in order to remove the SA induced by the high cooling rate of the simulation to the greatest possible extend. After relaxation, various constant uniaxial loads were applied to the simulation boxes for 300 ps. The instantaneous stress tensor E was controlled by the Hessian matrix H and an artificial matrix A using the following equation:

$$E = \frac{H \cdot A \cdot H^T}{V} \quad (1)$$

where V is the instantaneous volume of the simulation box.

According to the experimental results, the flow stresses of $\text{Cu}_{50}\text{Zr}_{50}$ and $\text{Cu}_{64.5}\text{Zr}_{35.5}$ bulk metallic glasses are approximately 1500 and 1700 MPa, respectively [16]. Furthermore, a recent MD simulation work showed that permanent deformation of a $\text{Cu}_{65}\text{Zr}_{35}$ MG can be resulted when it was subjected to a stress in the vicinity of flow stress at room temperature [17]. Therefore, the maximum applied loads to the $\text{Cu}_{50}\text{Zr}_{50}$ and $\text{Cu}_{64.5}\text{Zr}_{35.5}$ MGs in this work are 1300 and 1500 MPa, respectively, which is 200 MPa below the flow stresses of these materials. This is to eliminate the effects of anelasticity or low temperature creep to the highest extend. In fact, it is found that all the simulation boxes under each applied load in this study are able to recover to their original geometry within 300–500 ps after the applied loads are removed.

The construction of the FT matrix F is based on the nearest neighbor analysis of the structures, i.e. if two atoms are nearest neighbors, a pair of normal unit vectors \mathbf{n} can be constructed at the contact point. The relationship between F and \mathbf{n} is $F = \langle \mathbf{n} \otimes \mathbf{n} \rangle$, where the notation \otimes means the tensor product and the $\langle \rangle$ stands for the average over all vectors \mathbf{n} . The FT can be characterized by its three eigenvalues, λ_i ($i = 1, 2, 3$). Since the trace of F is unity, or equivalently, the sum of all the three eigenvalues is unity, thus, all the eigenvalues are equal to 1/3 for a perfect isotropic material. However, for an anisotropic material, a deviation of the eigenvalues from 1/3 can be measured or calculated. In this case, the anisotropic coefficient, α , can be defined as:

$$\alpha = \frac{3}{\sqrt{6}} \left(\sum_{i=1}^3 \left(\lambda_i - \frac{1}{3} \right)^2 \right)^{1/2} \quad (2)$$

It can be easily seen that α is zero for an isotropic material, whereas α is unity in the case of full anisotropy.

3. Results and discussions

The total and partial pair correlation functions (PCFs) of the simulated $\text{Cu}_{50}\text{Zr}_{50}$ and $\text{Cu}_{64.5}\text{Zr}_{35.5}$ MGs are shown in Fig. 1 together with the total PCF measured by synchrotron diffraction reported in Ref [16]. It can be seen that the PCFs obtained by the MD simulation are comparable with the experimental ones. Nevertheless, the small shoulder in the right part of the first maximum of the simulated total PCF is not so pronounced as the experimental one. According to Almyras, the small shoulder is mostly correlated to Zr–Zr and Cu–Zr superclusters composed by 20 and 31 atoms, respectively [18]. The undistinguished shoulder in this work is probably due to the fast quenching used in the MD simulation, where the short range order associated with small clusters had

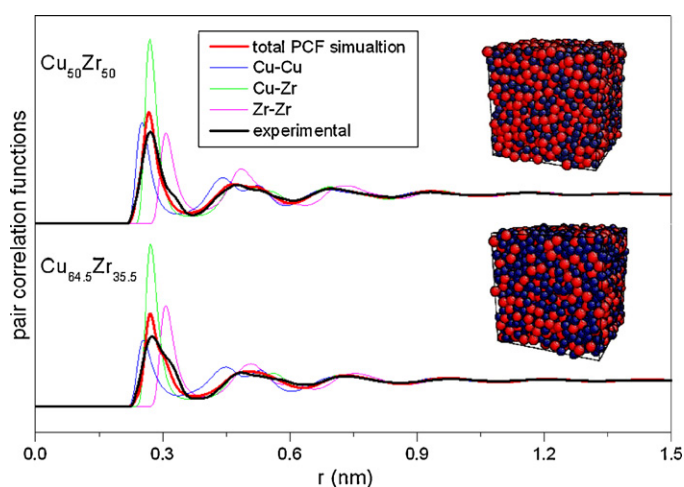


Fig. 1. The total and partial PCFs of the simulated $\text{Cu}_{50}\text{Zr}_{50}$ and $\text{Cu}_{64.5}\text{Zr}_{35.5}$ after relaxation at 300 K altogether with the experimental total PCF (solid black lines). The insets are the snapshots of the simulation boxes before deformation. The red and blue atoms are Zr and Cu, respectively. (For interpretation of the references to color in this figure legend, the reader is referred to the web version of the article.)

not enough time to develop the medium range order with superclusters. The volume of the simulated $\text{Cu}_{50}\text{Zr}_{50}$ and $\text{Cu}_{64.5}\text{Zr}_{35.5}$ MGs as a function of the temperature during the cooling process is shown in Fig. 2. The glass transition temperatures of the simulated $\text{Cu}_{50}\text{Zr}_{50}$ and $\text{Cu}_{64.5}\text{Zr}_{35.5}$ MGs are determined to be 691.6 and 660.5 K, respectively. Nevertheless, the glass transitions of $\text{Cu}_{50}\text{Zr}_{50}$ and $\text{Cu}_{64.5}\text{Zr}_{35.5}$ MGs are usually observed at about 670 and 616 K using differential calorimetric measurements (DSC) [19]. Comparing with the experimental results, the glass transition of the both simulated systems occurs at slightly higher temperature, which is most likely due to the high quenching rate used in the simulation.

The anisotropic coefficients of the simulated $\text{Cu}_{50}\text{Zr}_{50}$ and $\text{Cu}_{64.5}\text{Zr}_{35.5}$ MGs under various loads are calculated using Eq. (2) and are demonstrated in Fig. 3. The error bars are obtained by averaging all the α values at each simulation time step. It can be observed that the α values of both $\text{Cu}_{50}\text{Zr}_{50}$ and $\text{Cu}_{64.5}\text{Zr}_{35.5}$ increase with the applied loads, or equivalently, with the elastic strains. The α values of the $\text{Cu}_{64.5}\text{Zr}_{35.5}$ are slightly larger than those of the $\text{Cu}_{50}\text{Zr}_{50}$ under the same applied load. It can also be identified that tensile load and compressive load induce almost the same degree of SA in $\text{Cu}_{50}\text{Zr}_{50}$ and $\text{Cu}_{64.5}\text{Zr}_{35.5}$ when the applied

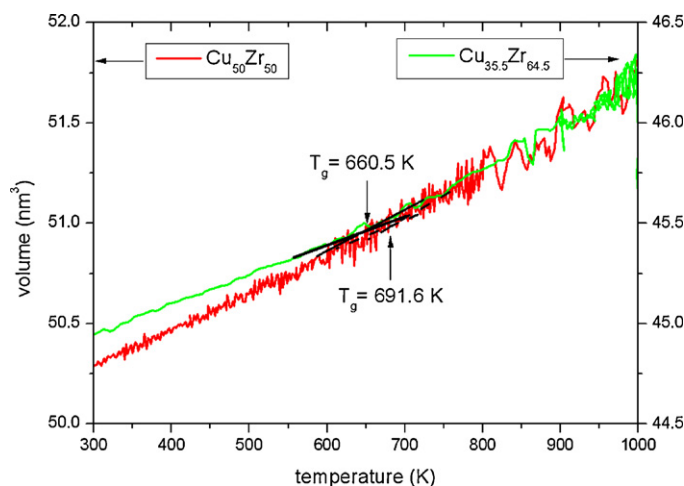


Fig. 2. The volume evolution of the simulated $\text{Cu}_{50}\text{Zr}_{50}$ (left) and $\text{Cu}_{64.5}\text{Zr}_{35.5}$ (right) MGs with temperature during the cooling process.

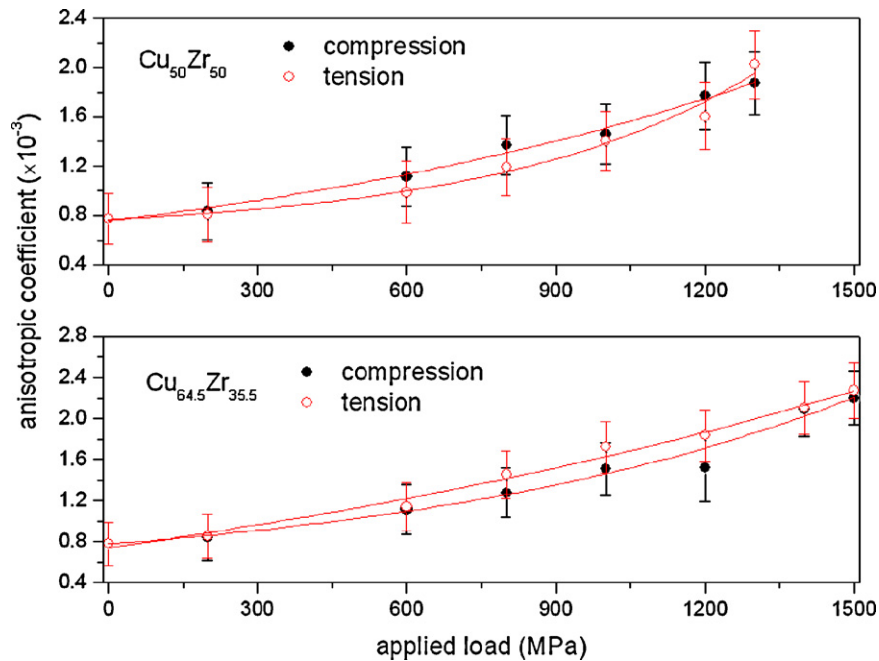


Fig. 3. The anisotropic coefficients of the simulated $\text{Cu}_{50}\text{Zr}_{50}$ and $\text{Cu}_{64.5}\text{Zr}_{35.5}$ MGs under compressive and tensile loads. The calculated values of the anisotropic coefficient are represented by the open and closed symbols. The red solid line is the fitting of the results using Eq. (3). (For interpretation of the references to color in this figure legend, the reader is referred to the web version of the article.)

load is below 200 MPa. However, when the applied load exceeds 200 MPa, larger α values in $\text{Cu}_{64.5}\text{Zr}_{35.5}$ are found under tensile load than under compressive load. Whereas the SA induced by tensile load is smaller than compressive load until 1200 MPa is reached in $\text{Cu}_{50}\text{Zr}_{50}$. It has been shown that α tends to reach some saturated values in amorphous silica after plastic deformation intervenes [8]. However, it is found in this work that α as a function of the applied load within the elastic range are best fitted using an exponential growth function of the following form:

$$\alpha = \alpha_0 + A \cdot \exp\left(\frac{-P}{B}\right) \quad (3)$$

where P is the applied load, α_0 , A and B are fitting parameters.

The values of α_0 , A and B obtained by fitting are listed in Table 1. Larger A values and smaller B values can be found in the tensile load mode in both $\text{Cu}_{50}\text{Zr}_{50}$ and $\text{Cu}_{64.5}\text{Zr}_{35.5}$. It can be seen that (1) the SA induced in both $\text{Cu}_{50}\text{Zr}_{50}$ and $\text{Cu}_{64.5}\text{Zr}_{35.5}$ by compressive and tensile loads are almost the same when the applied load is below 200 MPa; (2) under the loads from 600 to 1200 MPa, the SA induced by tensile loads is larger than by compressive loads in $\text{Cu}_{50}\text{Zr}_{50}$, whereas the opposite tendency is observed in $\text{Cu}_{64.5}\text{Zr}_{35.5}$; (3) tensile loads induce larger SA than compressive loads as the loads exceed 1200 MPa in both $\text{Cu}_{50}\text{Zr}_{50}$ and $\text{Cu}_{64.5}\text{Zr}_{35.5}$.

The contributions of different atomic pairs to the SA in $\text{Cu}_{50}\text{Zr}_{50}$ and $\text{Cu}_{64.5}\text{Zr}_{35.5}$ MGs have been studied by decomposition of the experimental total PCF using two Gaussian functions [6]. Nevertheless, the Cu–Cu and Cu–Zr pairs cannot be exactly separated due to high overlap of these two partial PCFs. In order to reveal the contributions of different atomic pairs to SA in more details, the partial anisotropic coefficients of the Zr–Zr, Zr–Cu and Cu–Cu pairs of the

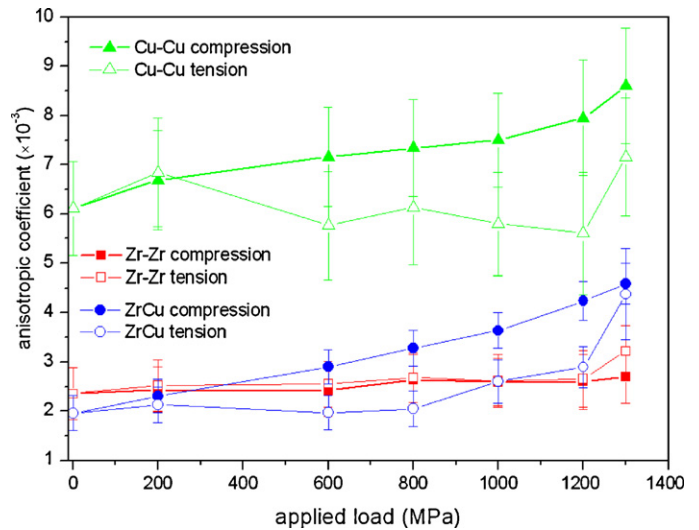


Fig. 4. The anisotropic coefficients of the Zr–Zr (red), Zr–Cu (blue) and the Cu–Cu (green) atomic pairs in the simulated $\text{Cu}_{50}\text{Zr}_{50}$ MGs under various tensile and compressive loads. (For interpretation of the references to color in this figure legend, the reader is referred to the web version of the article.)

simulated $\text{Cu}_{50}\text{Zr}_{50}$ and $\text{Cu}_{64.5}\text{Zr}_{35.5}$ MGs were calculated and the results are illustrated in Figs. 4 and 5, respectively. The error bars are derived using the same method as those shown in Fig. 3. It can be clearly seen that the initial α values of the Zr–Zr and Zr–Cu pairs in $\text{Cu}_{50}\text{Zr}_{50}$ are almost the same, whereas the initial α value of the

Table 1
The fitting results of the anisotropic coefficient as a function of the applied load using Eq. (3).

Materials	Load mode	α_0	A	B
$\text{Cu}_{50}\text{Zr}_{50}$	Compression	$(6.7 \pm 0.9) \times 10^{-4}$	$(1.0 \pm 0.6) \times 10^{-4}$	-515.7 ± 106.3
	Tension	$(1.3 \pm 0.3) \times 10^{-4}$	$(6.2 \pm 0.3) \times 10^{-4}$	-1259.8 ± 395.2
$\text{Cu}_{64.5}\text{Zr}_{35.5}$	Compression	$(4.3 \pm 0.2) \times 10^{-4}$	$(3.4 \pm 0.2) \times 10^{-4}$	-915.3 ± 239.6
	Tension	$(6.3 \pm 0.8) \times 10^{-4}$	$(13.7 \pm 1.0) \times 10^{-4}$	-2009.2 ± 622.2

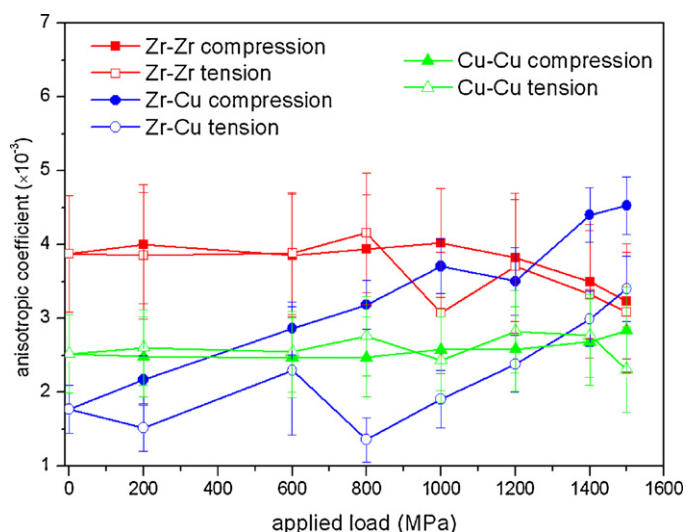


Fig. 5. The anisotropic coefficients of the Zr–Zr (red), Zr–Cu (blue) and the Cu–Cu (green) atomic pairs in the simulated $\text{Cu}_{64.5}\text{Zr}_{35.5}$ MGs under various tensile and compressive loads. (For interpretation of the references to color in this figure legend, the reader is referred to the web version of the article.)

Cu–Cu pair is about two times larger than these two pairs. The α values of the Zr–Zr pair is almost constant under both tensile and compressive loads below 1200 MPa. A slight increase in α of Zr–Zr pair can only be observed under the tensile load of 1300 MPa. The α values of Zr–Cu and Cu–Cu pairs increase monotonously with the applied compressive, whereas they first fluctuate around their initial values and then increase under large applied loads. Comparing with $\text{Cu}_{50}\text{Zr}_{50}$, the same behavior of the increase in the α values of Zr–Cu pair in $\text{Cu}_{64.5}\text{Zr}_{35.5}$ can be observed. Nevertheless, some major differences between the simulated $\text{Cu}_{64.5}\text{Zr}_{35.5}$ and $\text{Cu}_{50}\text{Zr}_{50}$ can be clearly observed: (1) the Zr–Zr pair was found to have the largest initial α value in $\text{Cu}_{64.5}\text{Zr}_{35.5}$ and a slight decrease in α values can be seen under both tensile and compressive loads. (2) The fluctuation in the α value of the Cu–Cu pair in $\text{Cu}_{64.5}\text{Zr}_{35.5}$ is much smaller than that in $\text{Cu}_{50}\text{Zr}_{50}$ and is almost constant under all the tensile and compressive loads. Based on the above results, it can be concluded that the Zr–Cu pair contributes the most to SA in $\text{Cu}_{64.5}\text{Zr}_{35.5}$ MG under both tensile and compressive loads, whereas the SA in $\text{Cu}_{50}\text{Zr}_{50}$ MG under both tensile and compressive loads can be attributed to inhomogeneous distribution of both Zr–Cu and Cu–Cu pairs. The different evolution of α with tensile and compressive load implies that different deformation mechanisms can exist in both $\text{Cu}_{50}\text{Zr}_{50}$ and $\text{Cu}_{64.5}\text{Zr}_{35.5}$ MGs between these two loading modes. Therefore, the structural evolution and the dynamics of

$\text{Cu}_{50}\text{Zr}_{50}$ and $\text{Cu}_{64.5}\text{Zr}_{35.5}$ MGs under static tensile and compressive loads are worthy to be further investigated.

4. Conclusions

In summary, the structural anisotropy in both $\text{Cu}_{50}\text{Zr}_{50}$ and $\text{Cu}_{64.5}\text{Zr}_{35.5}$ metallic glasses induced by static uniaxial tensile and compressive loads within the elastic regime can be clearly characterized using the second order contact fabric tensor. It is found that the degree of anisotropy within the elastic regime increases with the applied load following an exponential growth function. The most part of the structural anisotropy can be attributed to the Zr–Cu atomic pairs in $\text{Cu}_{64.5}\text{Zr}_{35.5}$ and Zr–Cu, Cu–Cu atomic pairs in $\text{Cu}_{50}\text{Zr}_{50}$. The evolution of the structural anisotropy associated with the Zr–Zr and Cu–Cu pairs implies that the deformation mechanism and the dynamics of $\text{Cu}_{50}\text{Zr}_{50}$ and $\text{Cu}_{64.5}\text{Zr}_{35.5}$ metallic glasses under compressive loads may be quite different from those under tensile loads.

Acknowledgement

Y. Zhang would like to acknowledge Dr. G. Wang and J. Tan for the valuable discussions on the simulation results and the data analysis.

References

- [1] Y. Suzuki, J. Haimovich, T. Egami, Phys. Rev. B 35 (1987) 2162–2168.
- [2] W. Dmowski, T. Egami, J. Mater. Res. 22 (2007) 412–418.
- [3] Á. Révész, E. Schafner, Z. Kovács, Appl. Phys. Lett. 92 (2008) 011910.
- [4] F. Spaepen, Acta Metal. 25 (1977) 407–415.
- [5] M.W. Chen, Annu. Rev. Mater. Res. 38 (2008) 445–469.
- [6] N. Mattern, J. Bednarčík, S. Pauly, G. Wang, J. Das, J. Eckert, Acta Mater. 57 (2009) 4133–4139.
- [7] X.D. Wang, S. Yin, Q.P. Cao, J.Z. Jiang, H. Franz, Z.H. Jin, Appl. Phys. Lett. 92 (2008) 011902.
- [8] Y.L. Sun, J. Shen, A.A. Valladares, J. Appl. Phys. 106 (2009) 073520.
- [9] S. Ogata, F. Shimizu, J. Li, M. Wakeda, Y. Shibutani, Intermetallics 14 (2006) 1033–1037.
- [10] Z.D. Sha, B. Xu, L. Shen, A.H. Zhang, Y.P. Feng, Y. Li, J. Appl. Phys. 107 (2010) 063508.
- [11] M.I. Mendeleev, M.J. Kramer, R.T. Ott, D.J. Sordelet, Philos. Mag. 89 (2009) 109–126.
- [12] G. Duan, D.H. Xu, Q. Zhang, G.Y. Zhang, T. Cagin, W.L. Johnson, W.A. Goddard, Phys. Rev. B 71 (2005) 224208.
- [13] T. Tomida, E. Egami, Phys. Rev. B 48 (1993) 3048–3057.
- [14] C.L. Rountree, D. Vandembroucq, M. Talamali, E. Bouchaud, S. Roux, Phys. Rev. Lett. 102 (2009) 195501.
- [15] Y.M. Kim, B.J. Lee, J. Mater. Res. 23 (2008) 1095–1104.
- [16] G. Wang, N. Mattern, S. Pauly, J. Bednarčík, J. Eckert, Appl. Phys. Lett. 95 (2009) 251906.
- [17] S.C. Lee, C.M. Lee, J.C. Lee, H.J. Kim, Y. Shibutani, E. Fleury, M.L. Falk, Appl. Phys. Lett. 92 (2008) 151906.
- [18] G.A. Almyras, Ch.E. Lekka, N. Mattern, G.A. Evangelakis, Scripta Mater. 62 (2010) 33–36.
- [19] W.H. Wang, J. Appl. Phys. 99 (2006) 093506.